



**QUEEN'S
UNIVERSITY
BELFAST**

Tip leakage flow and heat transfer on turbine blade tip and casing, Part 1: Effect of tip clearance height and rotation speed

Rahman, M. H., Kim, S. I., & Hassan, I. (2013). Tip leakage flow and heat transfer on turbine blade tip and casing, Part 1: Effect of tip clearance height and rotation speed. *International Journal for Computational Methods in Engineering Science and Mechanics*, 14(4), 290-303. <https://doi.org/10.1080/15502287.2012.725800>

Published in:

International Journal for Computational Methods in Engineering Science and Mechanics

Document Version:

Peer reviewed version

Queen's University Belfast - Research Portal:

[Link to publication record in Queen's University Belfast Research Portal](#)

Publisher rights

© 2013 Taylor & Francis Group, LLC

This is an Accepted Manuscript of an article published by Taylor & Francis in International Journal for Computational Methods in Engineering Science and Mechanics on 06 May 2013, available online: <http://www.tandfonline.com/doi/abs/10.1080/15502287.2012.725800>

General rights

Copyright for the publications made accessible via the Queen's University Belfast Research Portal is retained by the author(s) and / or other copyright owners and it is a condition of accessing these publications that users recognise and abide by the legal requirements associated with these rights.

Take down policy

The Research Portal is Queen's institutional repository that provides access to Queen's research output. Every effort has been made to ensure that content in the Research Portal does not infringe any person's rights, or applicable UK laws. If you discover content in the Research Portal that you believe breaches copyright or violates any law, please contact openaccess@qub.ac.uk.

Tip Leakage Flow and Heat Transfer on Turbine Blade Tip and Casing, Part 1: Effect of Tip Clearance Height and Rotation Speed

Md Hamidur Rahman¹, Sung In Kim² and Ibrahim Hassan³
Concordia University, Montreal, Quebec, H3G 1M8, Canada

Steady simulations were performed to investigate tip leakage flow and heat transfer characteristics on the rotor blade tip and casing in a single stage gas turbine engine. A typical high-pressure gas turbine stage was modeled with a pressure ratio of 3.2. The predicted isentropic Mach number and adiabatic wall temperature on the casing showed good agreement with available experimental data under similar operating condition. The present numerical study focuses extensively on the effects of tip clearance heights and rotor rotational speeds on the blade tip and casing heat transfer characteristics. It was observed that the tip leakage flow structure is highly dependent on the height of the tip gap and the speed of the rotor. In all cases, the tip leakage flow was seen to separate and recirculate just around the corner of the pressure side of the blade tip. This region of re-circulating flow enlarges with increasing clearance heights. The separated leakage flow reattaches afterwards on the tip surface. Leakage flow reattachment was shown to enhance surface heat transfer at the tip. The interaction between tip leakage flow and secondary flows that is induced by the relative casing motion, is found to influence significantly the blade tip and casing heat transfer distribution. A region of critical heat transfer exists on the casing near the blade tip leading edge and along the pressure side edge for all the clearance heights that were investigated. At high rotation speed, the region of critical heat transfer tends to move towards the trailing edge due to the change in inflow angle.

Nomenclature

C = chord at the blade tip, m

¹ Islamic University of Technology, Board Bazar, Gazipur, Bangladesh.

² School of Mechanical and Aerospace Engineering, Queen's University Belfast, UK.

³ Department of Mechanical and Industrial Engineering, ibrahim.hassan@concordia.ca.

- C_x = axial chord at the blade tip, m
 h = heat transfer coefficient, $\left(h = \frac{q}{T_w - T_{or.in}} \right)$, W/m²K
 i = incidence angle, $i = \beta_1 - \beta_1^0$
 PS = pressure side
 SS = suction side
 Nu = Nusselt number, $\left(Nu = \frac{hC}{k_t} \right)$
 k_t = fluid thermal conductivity, W/m K
 q = heat flux, W/m²
 t_y = blade thickness, m
 T = temperature, K
 $T_{0,in}$ = vane inlet total temperature, K
 V = absolute velocity
 V_{bl} = rotational speed of rotor blade, ω
 W = relative velocity
 x = axial coordinate, m
 y = Cartesian coordinate oriented along the circumferential direction, m
 y^+ = nondimensional wall distance, $\rho u_y \nu / \mu$
 z = Cartesian coordinate oriented along the radial direction, m
 α_1 = angle of absolute rotor inlet velocity vector
 β_1 = angle of relative rotor inlet velocity vector
 ρ = density, kg/m³
 ω = angular velocity

Subscript

- w = wall condition
 o = total

r = rotor

in = inlet

Superscript

0 = zero incidence or design point

+ = positive incidence

- = negative incidence

I. Introduction

TURBINE inlet temperature is continuously increasing to increase efficiency and power of modern gas turbine engines. Consequently, turbine components are subjected to high thermal loads. The heat load is not uniform but rather concentrated in certain critical regions on turbine components. The turbine blade tip clearance region is one critical region that experiences a high thermal load. Blade tip leakage flow occurs as a result of the pressure difference between the pressure and suction surfaces of the blade, and enhances heat transfer on the blade tip and casing.

Many experimental and numerical studies have been conducted to explore the details of the aerodynamics and heat transfer inside the turbine blade tip clearance. Unfortunately, due to the geometric complexity of the tip clearance and limitations in current measurement techniques, it is very difficult to capture accurate data in the tip gap region. Turbine linear cascades have been mainly used to study the fundamental characteristics of the tip leakage flow and the heat transfer on blade tip and casing, disregarding the rotational effect on the flow structure and heat transfer.

Ameri et al. (1998) conducted a numerical study of rotor heat transfer and stage efficiency for the GE- E^3 turbine blade. Three different configurations of the squealer tip geometry were investigated. Simulations were performed using the CFD code, TRAF3D.MB, designed for flows in complicated geometries. The computational grid consisted of hexahedral structured elements and a C-type grid around the airfoil surface. The speed of the rotor was set to 8450 RPM. The heat transfer analysis was conducted for a constant wall temperature (70% of the inlet total temperature). Flow separation appeared on the pressure side rim of the squealer cavity at 20% and 40% of the chord distance. A small vortex appeared near the pressure side cavity and a flow circulation zone was observed within the cavity space. The flow circulation zone blocks the flow in the tip clearance region, thereby, reducing the mass

transfer through the gap. Heat transfer distribution on the tip surface was also investigated and a higher heat transfer region near the pressure side of the flat tip surface was observed, and was attributed to leakage flow reattachment.

Tallman and Lakshminarayana (2001a) numerically studied the effect of the tip clearance height on the tip leakage flow in a linear cascade. 3D Navier-Stokes code with standard k- ϵ turbulence model was used. A high resolution H-grid was used with appropriate clustering near the wall ($y^+ < 10$). The clearance heights were 2.5% and 1% of the blade span. It was found that reducing tip clearance decreases greatly the mass flow rate through the gap, reduces the size of the leakage vortex and results in lower aerodynamic losses. The impact of the rotating relative motion of the turbine casing on the tip leakage flow was also investigated (Tallman and Lakshminarayana, 2001b). It was found that a developed shear layer at the wall, reduces the mass flow rate, and increases the flow blockage. Aerodynamic losses were higher due to the additional near-casing secondary flow.

A detailed experimental study of the heat transfer coefficient distribution on a gas turbine blade was conducted by Teng et al. (2001). A five-blade linear cascade was used in a low speed wind tunnel facility. Mainstream exit Reynolds Number was measured to be 5.3×10^5 . Three different tip clearance heights were investigated namely, 1.1%, 2% and 3% of the blade span. A critical region of high heat transfer was found at the mid chord of the blade tip surface near the pressure side, where a major pressure-driven leakage flow existed. Low heat transfer coefficients were obtained between the leading edge and the front of the suction side due to the entrance effect and the adverse pressure gradient on the mid-chord region of suction side tip. Larger tip gaps resulted in a higher overall heat transfer coefficient.

Mumic et al. (2004) conducted a numerical study of the leakage flow and heat transfer in the tip region for clearance heights of 1%, 1.5%, and 2.5% of the blade span. The total pressure and temperature at the rotor inlet were specified as 129.6 kPa and 297 K, respectively, and a pressure ratio of 1.22 was imposed across the blade. The uniform wall temperature of 350 K was used for heat transfer measurement. The overall heat transfer coefficient increased due to the increase in tip leakage flow velocity as the tip gap clearance increased. The flat tip heat transfer coefficient for reaches a peak value at mid-chord region along the pressure side due to leakage flow reattachment.

Key and Arts (2006) experimentally compared turbine tip leakage flow for flat and squealer tip geometries under high speed conditions. Flow visualization techniques helped analyze tip leakage flow structure in the tip gap and over the suction surface of the blade. Pressure ratio and tip flow velocity levels increased with increasing Reynolds number for the case of flat tip geometry. The highest pressure gradient across the blade tip occurred at around 6 to 8

percent of the axial chord. A pressure side separation vortex appeared at the tip of the blade in the case of a flat tip geometry, while no flow separation was present in the case of a squealer tip.

Newton et al. (2006) investigated the heat transfer and aerodynamics in a five-blade cascade for three different blade tip geometries; flat, suction side squealer and cavity squealer. Two tip clearance heights were also investigated; 1.6% and 2.8% of the blade span. Exit Reynolds number based on exit velocity and chord was measured to be 2.3×10^5 . For a flat tip, flow separated near the pressure edge and reattached on the tip surface. Heat transfer coefficient was measured on the suction surface and was found to be higher where the leakage vortex attaches on the suction surface.

The effect of tip clearance height and tip geometry on heat transfer and pressure losses was studied by El-Gabry (2007) numerically for an un-cooled gas turbine blade tip. The impact of blade tip geometry on the heat transfer distribution was investigated using three tip geometries namely, plain tip, full perimeter and partial perimeter squealer. A three-dimensional, compressible flow code named TACOMA was used. Three clearance heights equal to 1.25%, 2% and 2.75% of the blade span were also investigated. Numerical results showed that increasing the tip clearance increases the near tip pressure loading and consequently increases the tip leakage flow and the overall total pressure drop from the inlet to the exit of the blade. Increasing the tip gap increases the blade tip surface heat transfer for all three geometries. However, the relative motion of the rotor casing was disregarded.

From the above literature, the following key points could be summarized:

- Leakage flow separates near the pressure side edge and then reattaches on the tip surface, resulting in higher surface heat transfer.
- The leakage flow mass transfer rate and the size of the leakage vortex are dependent on the tip clearance height. A larger clearance height allows higher mass transfer rates and results in a larger leakage vortex.
- Higher tip leakage mass flow rate enhances the heat transfer on the blade tip and casing surfaces, since flow velocity increases with increasing temperature.
- The relative motion of the casing develops a boundary layer at the wall that opposes the leakage flow and reduces the strength of the leakage vortex.

Tip leakage flow is significantly affected by tip geometry and strongly related to heat transfer on the casing and blade tip surfaces. Both numerical and experimental studies were conducted using simplified flow conditions, such as, stationary blade, low pressure ratio, and low inlet temperature. Both steady and unsteady simulations of blade tip

leakage flow in a single stage gas turbine were performed by Phutthavong et al. (2008a, 2008b) using a non commercial CFD solver called Nistar. The shear stress transport (SST) $k - \omega$ turbulence model was selected in order to capture the flow characteristics in the tip gap region. CFD code validation and time-averaged simulations were presented in the first part, while the second part consisted of a time dependent and parametric study. In the present study, the former work is extended to include an investigation of heat transfer characteristics on the casing and tip surfaces associated with the tip leakage flow structure. The first part of the present study investigates the impact of tip clearance height and rotor speed on the heat transfer characteristics of the turbine blade tip and casing. The second part (Rahman et al. 2014) investigates stator-rotor interactions and their impact on the heat transfer characteristics.

II. Computational Details

Chana and Jones (2003) conducted an experimental study of turbine tip and casing heat transfer, using the Isentropic Light Piston Facility (ILPF) to test the MT1 turbine. The MT1 is a full-size, high-pressure, un-shrouded, one-stage research turbine. In the authors' research group, a full-size single stage gas turbine was modeled (Phutthavong et al., 2008a) based on the available limited information of the MT1 turbine (especially, the blade tip geometry in Chana and Jones, 2003). The turbine geometry is not identical to that of the MT1 turbine but its length is close to that of Chana and Jones (2003). The pitch angle was set to 12° for both the rotor and the stator to achieve an equal periodic angle. The turbine stage consisted of 30 vanes and 60 blades as opposed to 32 vanes and 60 blades in the MT1 turbine. The present study uses the same model as the one by Phutthavong et al. (2008). For comparison purposes, the boundary and operating conditions were based on the experimental works of Chana and Jones (2003) (see Table 1). A total pressure of 4.6 bars and a total temperature of 444 K were specified at the inlet of the stator domain, while a static pressure of 1.46 bar was set at the rotor domain outlet to achieve a value of static pressure at the blade exit as close as possible to the experimental one. A constant wall temperature boundary condition ($T_w = 222$ K) was imposed on the entire surface to compute the wall heat flux.

The present study uses a commercial CFD (Computational Fluid Dynamics) solver named ANSYS[®] CFX[®] R.11. High resolution second order central difference scheme was used to discretize the equations for the flow, turbulent kinetic energy, and specific dissipation rate. Krishnababu et al. (2007) generated numerical predictions for tip leakage flow and heat transfer using ANSYS CFX solver and different turbulence models: $k - \varepsilon$, $k - \omega$, and SST $k - \omega$ models. They found that the SST $k - \omega$ model shows the best agreement with experimental data. Hence, the

present study uses the SST $k - \omega$ turbulence model for turbulence closure. Ideal gas air was used as a working fluid. Gas properties (i.e. thermal conductivity, dynamic viscosity and specific heat at constant pressure) were set to be linear functions of temperature.

The computational domain consists of one vane and two rotor blades as shown in Fig. 1. The grid was generated using ANSYS® ICEM CFD™ grid generation tools. An unstructured tetrahedral grid with proper attention to the tip clearance region including blade tip and casing surfaces was adopted as shown in Fig. 2 for different cross-sectional planes. Grid clustering near the wall was performed by introducing prism layers to ensure sufficient number of cells within the tip clearance region.

Steady simulations were performed using the ANSYS CFX ‘Stage model’ option at the stator-rotor interface and allowed to run up to 500 iterations to reach at least three orders reduction of the residuals for continuity, momentum, heat transfer, and turbulence equations. Convergence of different parameters such as mass flow rate, total pressure, and static pressure at different locations of the domain were also monitored and remained constant over this large number of iterations. The ‘Stage model’ option in ANSYS CFX performs a circumferential averaging of the fluxes at the upstream side of the interface between the stator and rotor, then applies them as inlet boundary conditions to the rotor at the downstream side. All simulations were performed in a parallel processing environment which consisted of 10 processors on the High Performance Computing cluster system at Concordia University. Computation time was approximately 11 hours to achieve a converged steady-state solution within 500 iterations.

III. Comparisons and Grid Test

Numerical results obtained were compared with experimental data. The turbine length, blade chord, blade profile at the tip and root are same as those of Chana and Jones (2003). Boundary and operating conditions, based on the test conditions of Chana and Jones (2003), have been applied in this simulation (please refer to Table 1). The turbine inlet temperature and the rotor rotation speed are adopted from their experiments (Table 1). The isentropic Mach number at the stator exit casing and hub and the rotor inlet relative total pressure were compared with the experimental data (Table 2). Although the stator comprises 30 vanes, instead of 32 vanes, the present modeled vane has a larger exit angle and a narrower throat area (comparison of vane profiles at mid span). Hence, Mach number at vane exit is larger than that measured by Chana and Jones (2003).

One unsteady simulation was performed with an adiabatic wall condition. The predicted time averaged adiabatic wall temperatures on the casing surface were compared to experimental data as depicted in Fig. 3. The falling of the

adiabatic wall temperature at a fixed row of gages showed how the work extraction is distributed through the rotor passage. The predicted temperature distribution seems reasonable knowing that the experimental uncertainty of the adiabatic wall temperature was assessed to be ± 5 K. The pressure distributions on the vane and blade mid span are plotted in Fig. 4 and compared with available experimental (Hilditch et al., 1996) and numerical (Roux et al., 2001) data. Hilditch et al. (1996) and Roux et al. (2001) performed aerothermal measurements and predictions on NGV of the MT1 turbine. The test conditions were identical to those in the work of Chana and Jones (2003). The predicted location is slightly shifted to the trailing edge (Fig. 4a). In the present study, this trailing edge shock is under predicted with higher discrepancies (Fig. 4a) that might be attributed to the reflection of the vane trailing edge shock from the neighboring vane. When the flow enters the rotor section, it flows with a higher positive flow incidence caused by the stator vane, resulting in a high pressure gradient at the suction side of the leading edge, normal to the airfoil surface. As a result, the flow is separated from the blade wall at the suction side near the leading edge (Fig. 4b). The discrepancies in pressure distributions are not significant at all other locations. It was concluded that the gas turbine flow and heat transfer characteristics under the current operating conditions, representative of real engines conditions, can be well simulated using the present methodology.

Grid independence tests were conducted before obtaining any results, following two approaches. Firstly, pressure distributions at the rotor mid span were compared for one fine and one coarse grid of about 4×10^6 and 2.8×10^6 cells in the rotor domain, respectively. The two grids yielded very similar results. The percent difference between the static pressure values was less than 3%. Secondly, the velocity and temperature profiles in the tip region were compared for different number of cells in the tip clearance region (e.g. 20, 35, 45, 60 cells in radial direction, Fig. 5). Grids with 45 cells and 60 cells in the tip clearance yielded very similar results for both velocity and temperature profiles. Consequently, all analysis in the current study uses a coarse grid with 45 cells in the tip region, and the average y^+ on the tip and casing surfaces is less than 10.

IV. Results and Discussion

Details of heat transfer distributions on the blade tip and casing, associated with tip leakage aerodynamics in the blade tip clearance region are discussed in the subsequent sections. A tip clearance of 1.2 mm, a uniform inlet total temperature of 444 K, and a rotational speed of 9500 RPM were imposed for the Baseline case. The test matrix of all cases is shown in Table 3. The effects of clearance height were investigated by considering three gap sizes of 0.6 mm, 1.2 mm, and 2 mm (1.5%, 3%, and 5% of the blade span, respectively). Similarly, the effect of rotor rotational

speed on the leakage flow structure and its influence on the heat transfer distributions was investigated by considering three different rotor speeds namely 9500 RPM (off-design; 76% of design speed), 12500 RPM (design speed), and 15500 RPM (off-design; 124% of design speed). Typical rotating speeds of gas turbines range between -30% and 20% of the design speed (Krieger et al., 1999). The lower rotor speed (9500 RPM) corresponds to the experimental reference, the same interval was applied to obtain the higher speed (15500 RPM). Leakage flow structure variation is significantly affected by clearance heights and rotational speeds (incidence angle), and influences the distribution of heat transfer rate. The present study focuses extensively on the aerodynamics and heat transfer characteristics. It is to mention that all results are presented in a rotating frame of reference.

Typical flow structure taking place in the tip clearance region was sketched in Fig. 6a. The no slip condition on the blade tip and the constant relative motion of the casing in a direction opposite to that of the tip leakage flow create a complex tip clearance viscous flow field. Leakage flow entering the tip gap from the pressure side with sudden change in area and direction causes flow separation (SB) from the blade tip surface. Leakage flow then reattaches on the tip surface (LR) beyond SB. The outer casing velocity V_{casing} shears the outer edge of the tip leakage flow in the gap. It follows that there must be a stagnation line S1-S2 on which the velocity is zero. The relative flow (RR) with respect to the blade tip is reversed near the casing. The relative casing motion is communicated to the leakage flow via viscous and turbulent diffusion process. Moreover, the relative casing motion may help in reducing the tip leakage mass flow rate and momentum by shearing it in its opposite direction (Arts, 2004).

Figure 6b presents a 3-D view of path lines to help visualize the complex tip leakage flow structure. Path lines of the fluid particles are originated from two distinct locations. The first location is in the tip region where flow separates near the pressure side edge. The recirculating flow near the pressure side moves downstream with swirling motion along the tip surface. In all cases, this recirculation (SB) zone is observed on the blade tip surface. However, the strength and size of SB vary with operating and geometry conditions. The second location is taken from the passage flow near the casing. It shows a relative reverse flow (RR) near the casing and a vortical flow. The vortical flow moves downstream with a vortical mixing between RR and tip leakage flow, called the secondary reversed leakage vortex (SRLV). The strength of RR is fully dependent on the rotor speed. The details of the effect of the clearance height and rotor speed on the leakage flow structure and heat transfer are presented in the following sections.

A. Effect of the Tip Clearance Height

The variation of the tip leakage flow structure with clearance height is shown in Fig. 7 as streamlines. Since the casing and the tip leakage flow have mainly circumferential motions with opposing directions, the circumferential flow variation in the tip clearance region can be used to see their interaction. Tangential velocity profiles at several locations across the blade tip at 25% axial chord plane are plotted against the clearance height in Fig. 8. Separation bubble (SB) is an important flow phenomenon associated with the leakage flow and heat transfer. It results in a low pressure region on the blade tip surface near the pressure side, and obstructs the leakage flow attachment on the tip surface. The negative velocity near the blade tip surface in the vicinity of the pressure side, representing SB, can also be seen in Fig. 8. The height of SB increases with the size of the tip gap (Figs. 7 & 8). As the clearance height increases, the area of SB also enlarges. Leakage flow reattachment (LR) on the tip surface occurs around $y/t_y = 25%$ and $40%$ in $x/C_x = 25%$ plane for Case 1 (0.6 mm) and Baseline (1.2 mm), respectively. At Case 2 (2 mm), leakage flow reattaches at about $y/t_y = 70%$ from the pressure side edge at $x/C_x = 25%$ plane. LR increases the surface pressure and reduces the boundary layer thickness. Thus it is expected to have higher heat transfer at LR region.

It is also seen that the relative reverse flow (RR) is outstanding near the suction side. It restricts the leakage flow near the blade tip surface in the vicinity of the suction side. The effect of RR is gradually diminishing from suction side to pressure side, where it encounters the tip leakage flow from the pressure side. Under the same operating condition, the leakage flow velocity increases with the clearance height, thus mass transfer rate through the tip gap increases. The rate of RR also increases with the clearance height. However, it decreases in Case 2 because the leakage mass flow rate increases but the viscous effect on the casing remains invariable at the same rotation speed. The tip leakage flow, passing through the tip clearance, creates a tip leakage vortex along the suction side of the blade, causing significant aerodynamic losses by changing the rotor passage flow momentum. In Case 1, the tip leakage flow is too weak to generate a tip leakage vortex (see Fig. 8), whereas the tip leakage vortex becomes significant as the clearance height increases.

Figure 9 shows contours of Nusselt number on the casing for different clearance heights. The higher Nusselt number region is seen around the pressure side edge. Nusselt number is maximum near the blade leading edge and then decreases gradually. This higher heat transfer region coincides with the region where the blade loading driven tip leakage (BLL) of higher temperature from pressure side conflicts with the casing along the pressure side edge. It

is also observed that the Nusselt number is low in the region near the suction side of the blade, where the tip leakage flow is detached from the casing by RR (see Figs. 7 and 8). Nusselt number distributions on the blade tip surface are presented in Fig 10. Near the pressure side edge, heat transfer rate is lower indicating the region of flow recirculation on the tip surface for all cases (see Fig. 7). For 2 mm height, Nusselt number near the suction side, between 20% to 60% of the chord, is higher caused by the leakage flow reattachment beyond the flow separation region (Fig. 7). However, at smaller clearance heights, the region of low heat transfer rate appears again beyond the leakage flow reattachment region where the heat transfer rate is high. At all clearance heights, the heat transfer rate on the tip surface becomes the minimum value near the trailing edge because of leakage flow lift off and the coverage of recirculating flow.

Nusselt number distributions on the casing circumference (lines without symbol) are plotted for different clearance heights at $x/C_x=25\%$ in Fig. 11. Nusselt number on the casing is highest near the pressure side edge, as discussed earlier, and rapidly decreases along the circumferential direction. And then, it remains relatively low beyond locations of $y/t_y = 15\%$, 20% and 75% for 0.6 mm (Case 1), 1.2 mm (Baseline), and 2.0 mm (Case 2) heights, respectively. It can be attributed to RR coverage on the casing in this region (see Fig. 8). Figures 7 & 8 show that Case 1 has a weaker RR (lower velocity) coverage and SRLV close to the pressure side in the tip clearance region in comparison with Baseline case. The fluids inside the tip gap are fully mixed through SRLV, so the effect of RR coverage is not identified in temperature profiles in Fig. 12. Hence, Case 1 has a higher Nusselt number in this region (beyond $y/t_y = 20\%$) than the Baseline case (Fig. 11). The area of RR coverage is small for Case 2 due to the higher mass flow rate leakage flow. In this case, there is no SRLV in the tip region (Fig. 7c). This is the reason why Case 2 has larger distribution of high Nusselt number on the casing above the blade tip, up to around $y/t_y = 60\%$, as opposed to the cases with smaller tip gaps (Fig. 11).

Figure 11 also shows Nusselt number distributions (lines with symbols) along the circumferential line on the blade tip surface at $x/C_x=25\%$ for different clearance heights. Case 1 and Baseline have the same pattern of Nusselt number distributions. The low Nusselt number region, caused by SB, exists near the pressure side edge. Beyond this region, Nusselt number reaches a maximum due to LR on the tip surface. SRLV enhances the mixing between the tip leakage flow and RR in the tip clearance region (see Figs. 8 and 12). Therefore, heat transfer rate decreases again toward the suction side in Case 1 and Baseline case. However, the Nusselt number continuously increases from pressure side to suction side in Case 2, in contrast with the other cases. This is attributed to a larger SB from the

pressure side edge and LR close to the suction side edge without SRLV in the tip region (Fig. 7c). The key elements of the tip leakage flow structure such as, SB, RR and SRLV reduce the mass flow rate of tip leakage flow and the heat flux on the tip and casing. The size and position of them depend on the clearance height. Optimum height and tip geometry for maximizing the effect of RR, SB and SRLV could minimize the tip leakage loss and the thermal load on the tip and casing.

B. Effect of the Rotational Speed

To understand how the rotational speed alters the velocity triangle at the inlet of a rotor blade passage at off-design conditions, the velocity triangle and incidence angle are presented in Fig. 13a. Velocities V and W are the absolute and relative velocities, respectively. V_{bl} is the rotational velocity of the rotor blade, $r\omega$ (r =radius, ω =angular velocity). The superscripts of “-”, “0”, and “+” indicate negative, zero and positive incidences, respectively. The incidence angle, i , is defined as $(\beta_1 - \beta_1^0)$. Positive incidence means that the relative inlet flow angle, β_1 is larger than the blade inlet angle, β_1^0 . The flow path through the tip clearance region at different rotor speeds is also presented in Fig. 13 with streamlines originating from the same circumferential line upstream the rotor blade. The flow incidence angle changes from positive (Fig. 13b) to negative (Fig. 13d) with respect to rotor speeds. The blade tip region is covered by the blade loading driven tip leakage flow (BLL) from the pressure side when the rotor has a positive incidence angle (Baseline case, 9500 RPM). In this case, the most of BLL has a normal direction to the blade profile of pressure side edge. As a result, the separation bubble (SB) occurs along the pressure side edge (see Fig. 14a). In contrast to Baseline, the suction side tip leakage from leading edge incidence flow (SSL), mainly covers the upstream parts of the tip clearance region (near the leading edge) for Case 4 (15500 RPM; negative incidence). Therefore, SB near the pressure side edge becomes very small (see Fig. 14c) and not dominant up to 70% of axial chord. The small SB occurs near the leading edge and the suction side due to the negative incidence of SSL in Case 4 (see Fig. 17). The effect of rotational speed on the variation of the tip leakage flow structure for 1.2 mm clearance height is illustrated by using 2-D velocity vectors in Fig. 14. The relative reverse flow (RR) near the casing is significant and dominates in the tip clearance region as the rotation speed increases, because the effect of the relative casing motion increases with the rotation speed. It is also attributed to the change of flow incidence angle depending on the rotation speed. Leakage flow characteristics inside the tip gap are similar between Baseline

and Case 3 (12500 RPM) (Figs. 14a, b). However, when the rotor runs with a negative incidence (Case 4), the leakage flow structures and heat transfer distribution are very different from those in other cases.

To look into the effect of turbine rotational speed on its operating conditions, Table 4 is presented. It is seen that the change of speed causing the flow velocity and temperature change is obvious. However, it is important to check whether it has significant effect on the heat transfer and turbine performance. Effect of the increased turbine rotating speed on heat transfer into the blade tip and casing for the steady-state simulations can be seen in Table 5. When the turbine speed increases to 12500 RPM, the area-averaged heat fluxes on the casing decrease by 1.47%. However, there is a significant decrease of 12% of heat flux seen on the blade tip. As a result, blade material, more particularly the tip region, will require more cooling capacity to keep the same material temperature. Furthermore, the maximum heat flux on the casing is observed on the casing at 9500 RPM. The comparison of the turbine performance is also summarized in Table 6 for the cases of 9500 RPM and 12500 RPM. At a higher speed, both the total-to-total and total-to-static isentropic efficiency increased by 3.2% and 3.5%, respectively.

The Nusselt number distributions along the casing circumference are presented in Fig. 15 for the different rotor speeds. The effect of RR and flow incidence on heat transfer onto the casing with varying rotation speeds is well shown in Fig. 15. BLL is shifting toward the trailing edge due to the increase of SSL with the rotor speed (Fig. 13). As a result, the critical region of high heat transfer rate, caused by BLL along the pressure side edge, moves toward downstream trailing edge with increasing rotor speed. In Case 4, RR takes more space inside the tip gap because the effect of the relative motion on the casing is significantly strengthened. Therefore, the low heat transfer rate region due to RR coverage near the suction side is enlarged with the rotor speed. At 25% axial chord, the maximum Nusselt number of Baseline case (positive incidence) increases 20% from that of Case 3 (design speed). For a higher rotation speed (Case 4, negative incidence), the Nusselt number distribution at 25% axial chord is flattened, because the entire area is covered by the negative incidence flow (SSL) and RR (see Figs. 13c and 14c). In Case 4, Nusselt number is reduced by 20% from that of Case 3. The critical region of high heat transfer in Case 4 appears near the trailing edge where the Nusselt number increases 3% and 32% from Case 3 and Baseline, respectively.

Nusselt number distributions on the blade tip surface for different rotor speeds are presented in Fig. 16. In Case 3, there is a low Nusselt number region near the pressure side edge and trailing edge due to SB, and a high Nusselt number region because of LR (Figs. 10b and 16a). In Case 4, the heat transfer distribution is different from those of lower speed conditions due to different leakage flow structure. A higher Nusselt number region is presented near the

leading edge (Fig. 16b). A low Nusselt number region occurs in the intermediate region between 20% to 40% axial chord. This is attributed to the complex flow field and SRLV mixing of BLL from the pressure side, upstream SSL, and RR. Point A is located near the leading edge and has a higher Nusselt number, Point B is about 30% axial chord and near the pressure side (Fig. 16b). As mentioned earlier, in Case 4, a small recirculation zone in the streamwise direction occurs near the leading edge due to SSL, (negative u of A in Fig. 17). This inlet flow of SSL has a higher temperature profile (at point A in Fig. 18). The leakage flow of BLL from the pressure side starts occurring beyond 20% axial chord (Fig. 17). Eventually, SRLV is formed around 20% to 40% axial chord region, and leaves toward the blade suction side. It results in a low Nusselt number region along this SRLV passage. Beyond this region, the BLL occupies the tip surface. The tip leakage flow structure variations with the rotation speed have been observed with the heat transfer characteristics on the tip surface and the casing. As the incidence angle decreases from positive to negative values, the dominant tip leakage flow is changed from BLL to SSL. It contributes not only to the change in position and size of SB, RR and SRLV, but also to the variation of the critical heat transfer region. The relation between the heat transfer distribution and the incidence angle should be considered in turbine blade twist angle optimization.

V. Conclusions

Steady simulations were performed to investigate the relation between tip leakage flow pattern and the heat transfer distributions on the casing and blade tip surface. A high pressure ratio single stage turbine model was adopted in this study. The effect of different clearance heights and rotation rates of the blade were studied for both leakage flow aerodynamics and heat transfer. This work will assist the designer to identify the region of high thermal load on the tip surface and the casing with two major parameters such as tip clearance height and rotor rotation speed. The current analysis findings could be summarized as follows:

1. Tip leakage flow structure is highly dependent on the heights of the tip gap as well as rotor speeds. Flow separation (SB) occurs near the pressure side edge of the blade tip for all clearance heights. Low heat transfer rate is observed in the SB region.
2. The tip leakage flow reattachment (LR) on the tip surface tends to move towards the suction side as the clearance height increases. This LR contributes to the blade tip surface heat transfer enhancement.
3. The critical region of high heat transfer on the casing exists above the blade tip leading edge and along the pressure side edge at all clearance heights. However, at high rotation speeds it tends to move downstream

towards the trailing edge due to the change in flow incidence and the enhanced effect of casing relative motion.

4. The maximum Nusselt number on the casing, in the Baseline case (24% lower speed), increases by 20% compared to Case 3 (design speed). For Case 4 (24% higher speed), the Nusselt distribution is flattened, because the entire area is covered by the relative reverse flow (RR). The maximum Nusselt number reduction is about 22% of that in Case 3 at 25% axial chord plane. The critical region of high heat transfer for Case 4 appears close to the trailing edge where the Nusselt number on the casing at 75% axial chord plane increases 3% than Baseline case.
5. When the rotor speed increases, the suction side tip leakage from leading edge incidence flow (SSL) results in a higher Nusselt number in the blade tip leading edge region. The blade loading driven tip leakage flow (BLL) occurs in the middle region and then SRLV is formed. The lower Nusselt number distribution on the blade tip surface appears due to the SRLV mixing of SSL, BLL and RR.

References

- Ameri, A. A., Steinthorsson, E., and Rigby, D. L., "Effect of Squealer Tip on Rotor Heat Transfer and Efficiency", *Journal of Turbomachinery*, Vol. 120, pp. 753-759, 1998.
- Arts, T., "Turbine Blade Tip Design and Tip Clearance Treatment," *Von Karman Institute Lecture Series VKI LS 2004-02*, 2004.
- Chana, K. S., and Jones, T. V., "An Investigation on Turbine Tip and Shroud Heat Transfer," *Journal of Turbomachinery*, Vol. 125, pp. 513-520, 2003.
- El-Gabry, L. A., "Numerical Modeling of Heat Transfer and Pressure Losses for an Uncooled Gas Turbine Blade Tip: Effect of Tip Clearance and Tip Geometry," *Proceedings of ASME Turbo Expo 2007*, GT2007-27008, 2007.
- Hilditch, M. A., Smith, G. C., Anderson, S. J., Chana, K. S., Jones, T. V., Ainsworth, R. W. and Oldfield, M. L. G., "Unsteady Measurements in an Axial Flow Turbine," *AGARD Conference Proceeding* p.571, 1996.
- Key, N. L., and Arts, T., "Comparison of Turbine Tip Leakage Flow for Flat Tip and Squealer Tip Geometries at High-Speed Conditions," *Journal of Turbomachinery*, Vol. 128, pp. 213-220, 2006.
- Krieger, M. W., Lavoie, J. P., Vlastic, E. P., and Moustapha, S. H., "Off-Design Performance of a Single-Stage Transonic Turbine," *Journal of Turbomachinery*, Vol. 129, pp.177-183, 1999.
- Krishnababu, S. K., Newton, P. J., Dawes, W. N., Lock, G. D., Hodson, H. P., Hannis, J., and Whitney, C., "Aero-Thermal Investigations of Tip Leakage Flow In Axial Flow Turbines Part I: Effect of Tip Geometry and Tip Clearance Gap," *Proceedings of ASME Turbo Expo 2007*, GT2007-27954, 2007.
- Mumic, F., Eriksson, D., and Sunden, B., "On Prediction of Tip Leakage Flow and Heat Transfer in Gas Turbines," *Proceedings of ASME Turbo Expo 2004*, GT2004-53448, 2004.
- Newton, P. J., Lock, G. D., Krishnababu, S. K., Hodson, H., P., Dawes, W. N., Hannis, J., and Whitney, C., "Heat Transfer and Aerodynamics of Turbine Blade Tips in a Linear Cascade," *Journal of Turbomachinery*, Vol. 128, pp. 300-309, 2006.
- Phutthavong, P., Hassan, I., and Lucas, T., "Unsteady Numerical Investigation of Blade Tip Leakage, Part 1: Time-Averaged Results," *Journal of Thermophysics and Heat Transfer*, Vol. 22, No. 3, pp. 464-473, 2008a.
- Phutthavong, P., Hassan, I., and Lucas, T., "Unsteady Numerical Investigation of Blade Tip Leakage, Part 2: Time-Dependent Parametric Study," *Journal of Thermophysics and Heat Transfer*, Vol. 22, No. 3, pp. 474-484, 2008b.

- Rahman, M. H., Kim, S. I., and Hassan, I., "Tip Leakage Flow and Heat Transfer on Turbine Blade Tip and Casing: Effect of Unsteady Stator Rotor Interaction," in press, *Int. Journal of Computational Methods*, 2014.
- Roux, J. M., Mahé, P., Sauthier, B., and Duboué, J. M., "Aerothermal Predictions with Transition Models for High-Pressure Turbine Blades," *Proceedings of the Institution of Mechanical Engineers, Part A: Journal of Power and Energy*, Vol. 215, pp.735-742, 2001.
- Tallman, J., and Lakshminarayana, B., "Numerical Simulation of Tip Leakage Flows in Axial Flow Turbines, With Emphasis on Flow Physics: Part I–Effect of Tip Clearance Height," *Journal of Turbomachinery*, Vol. 123, pp.314-323, 2001a.
- Tallman, J., and Lakshminarayana, B., "Numerical Simulation of Tip Leakage Flows in Axial Flow Turbines, With Emphasis on Flow Physics: Part II–Effect of Outer Casing Relative Motion," *Journal of Turbomachinery*, Vol. 123, pp.324-333, 2001b.
- Teng, S., Han, J-C., and Azad, G. M. S., "Detailed Heat Transfer Coefficient Distributions on a Large-Scale Gas Turbine Blade Tip," *Journal of Heat Transfer*, Vol. 123, pp.803-809, 2001.

Table 1 Modeled turbine geometry and test conditions

	Baseline case	Experiments (Chana and Jones, 2003)
Turbine inlet temperature, K	444	444
Stator inlet total pressure, bar	4.6	4.6
Rotor exit static pressure, bar	1.43	1.428 (hub) 1.435 (casing)
Rotor rotation speed, RPM	9500	9500
Blade tip geometry	Flat tip	Flat tip
Number of stator vanes	30	32
Number of rotor blades	60	60

Table 2 Comparison with the experimental data

Parameter, Location	Present (adiabatic)	Experiments (Chana and Jones, 2003)
Isentropic Mach number at NGV exit (hub)	1.24	1.034
Isentropic Mach number at NGV exit (casing)	1.0665	0.925
Relative total pressure at rotor inlet, bar	2.571	2.7

Table 3 Test matrix of parametric study

Test matrix	Case number	Tip clearance, mm (% of blade span)	Rotor speed, RPM
Effect of tip clearance height	Baseline	1.2 (3)	9500 (24% lower)
	1	0.6 (1.5)	9500
	2	2 (5)	9500
Effect of rotor rotation speed	3	1.2	12500 (design speed)
	4	1.2	15500 (24% higher)

Table 4 Change of operating conditions due to speed change

Cases	T _{inlet}	Pressure Ratio	Rotor speed, RPM	Av. Vel. Stator exit	Av. Temp. Stator exit	Mass flow
Case 3 (12500 RPM)	444 K	3.15	12500	394 m/s	359.6 K	0.3902 kg/s
Baseline (9500 RPM)	444 K	3.15	9500	412 m/s	352.5 K	0.3909 kg/s

Table 5 The turbine heat transfer characteristics

Cases	Steady area-av. q, casing	Steady area-av. q, tip	Steady max q, casing	Steady max q, tip
Baseline (9500 RPM)	203,655 W/m ²	285,716 W/m ²	722,528 W/m ²	565,396 W/m ²
Case 3 (12500 RPM)	206,688 W/m ²	254,626 W/m ²	709,133 W/m ²	576,566 W/m ²
Cases	Steady area-av. h, casing	Steady area-av. h, tip	Steady max h, casing	Steady max h, tip
Baseline (9500 RPM)	7,364 W/m ² K	3,896 W/m ² K	8,357 W/m ² K	5,677 W/m ² K
Case 3 (12500 RPM)	7,385 W/m ² K	3,901 W/m ² K	8,404 W/m ² K	5,579 W/m ² K

Table 6 The turbine performance characteristics

Cases	Power output	T-T isentropic efficiency	T-S isentropic efficiency
Case 3 (12500 RPM)	1.128 MW	0.967	0.886
Baseline (9500 RPM)	1.086 MW	0.935	0.851

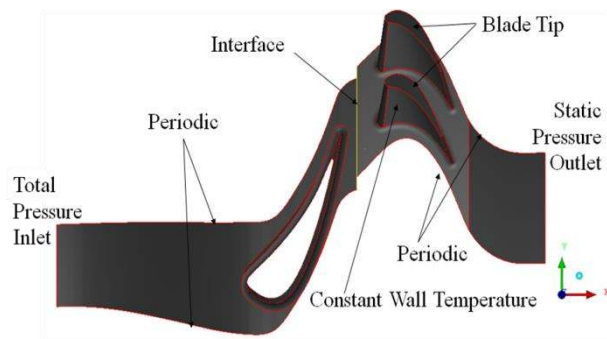
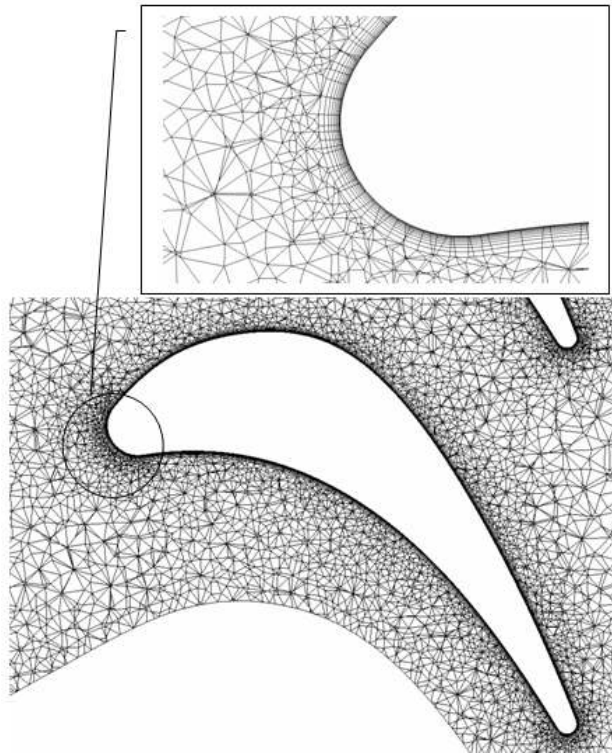
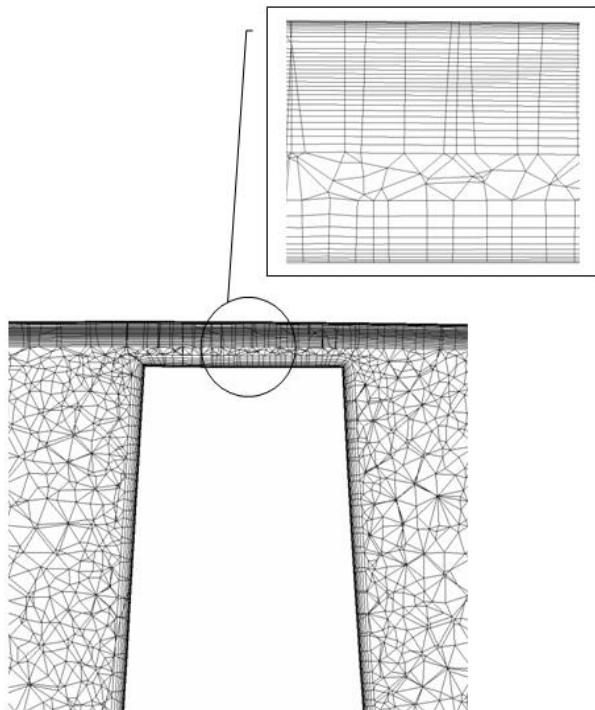


Figure 1. Computational domain with one stator and two rotor blades.



(a)



(b)

Figure 2. Computational grid at (a) rotor mid span. (b) stream wise location showing grid resolution in the tip clearance region.

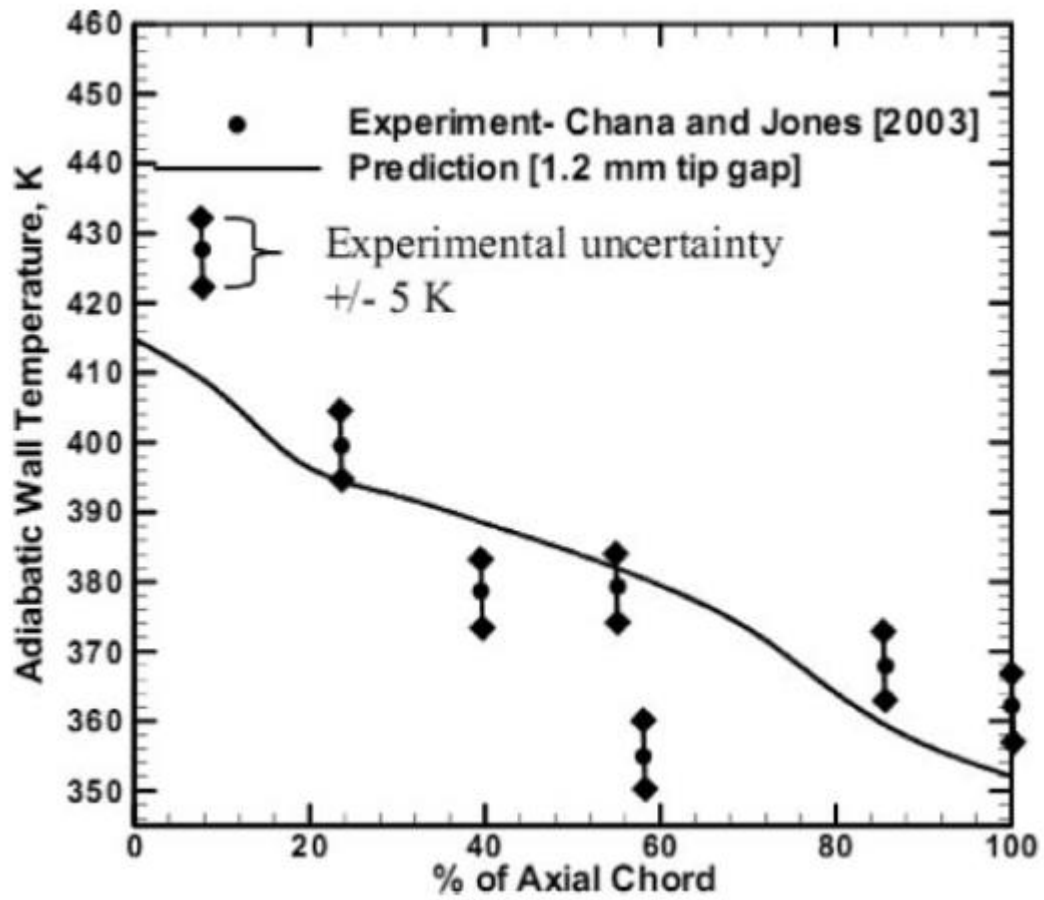
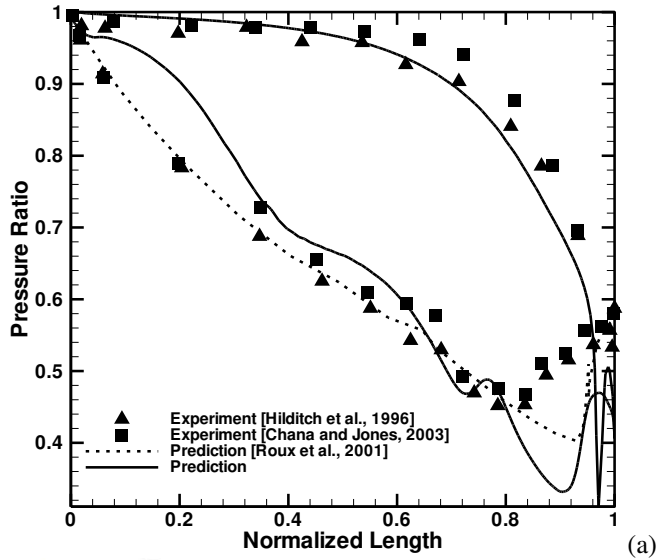
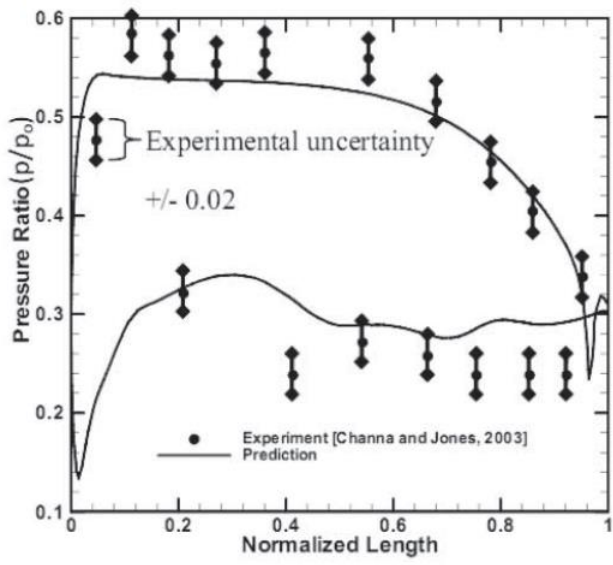


Figure 3. Comparison of averaged adiabatic wall temperature on the casing from blade tip leading to trailing edge (Baseline case).

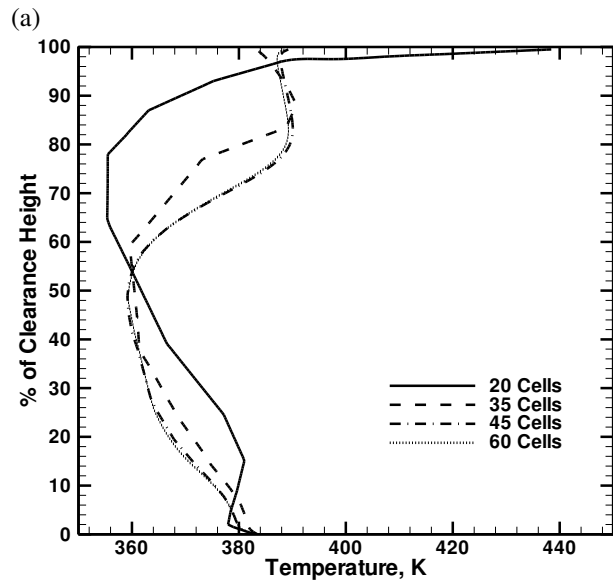
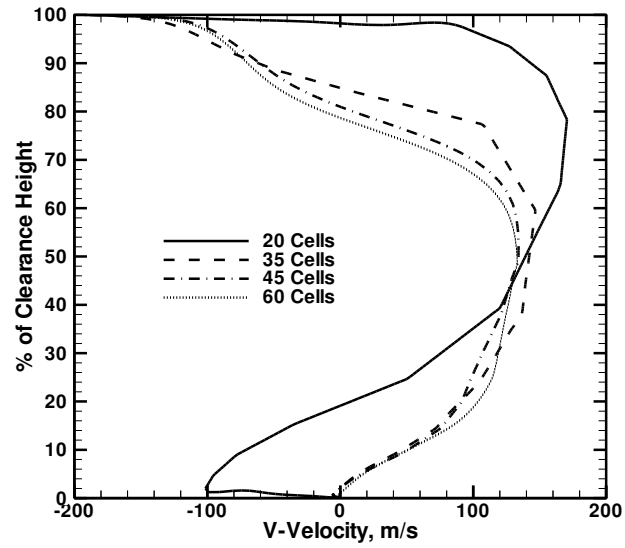


(a)



(b)

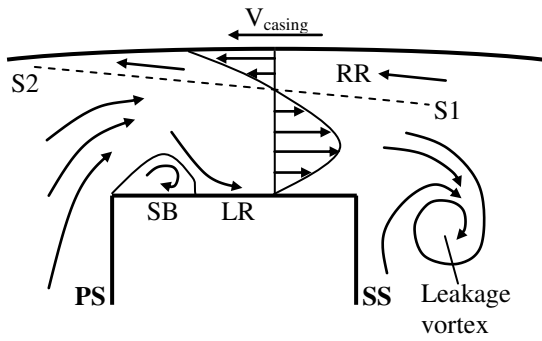
Figure 4. Comparison of predicted static pressure distribution at (a) the stator and (b) the rotor mid span (Baseline case; 9500 RPM).



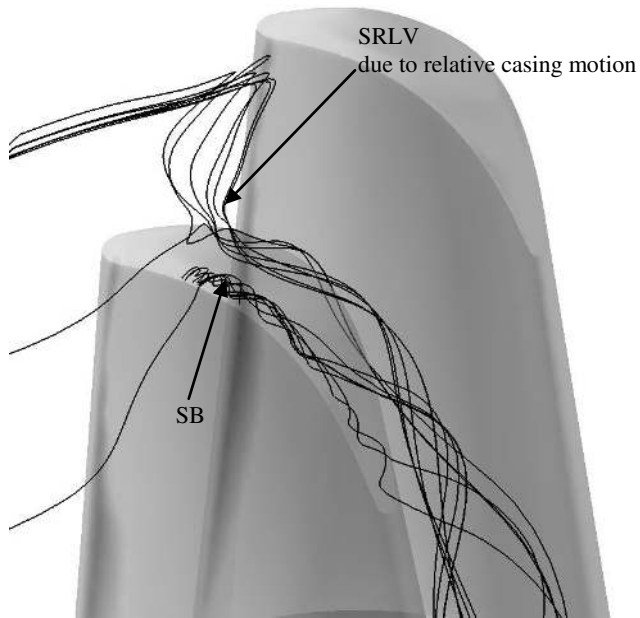
(a)

(b)

Figure 5. Effect of number of cells in the tip clearance region on (a) V-velocity profile and (b) Static temperature profiles (Baseline case, 9500 RPM).



(a) Schematic of the typical tip leakage flow structure (flow observed from a rotating frame of reference)



(b) Pathlines in the tip clearance region (Baseline case, 9500 RPM)

Figure 6. The tip leakage flow structures.

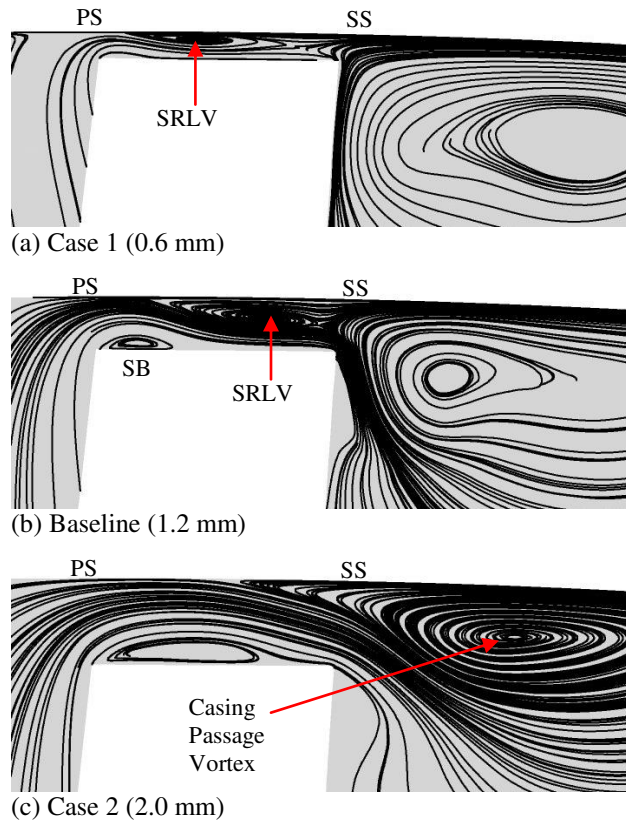


Figure 7. Streamlines for the tip leakage flow structures at the 25% axial chord plane.

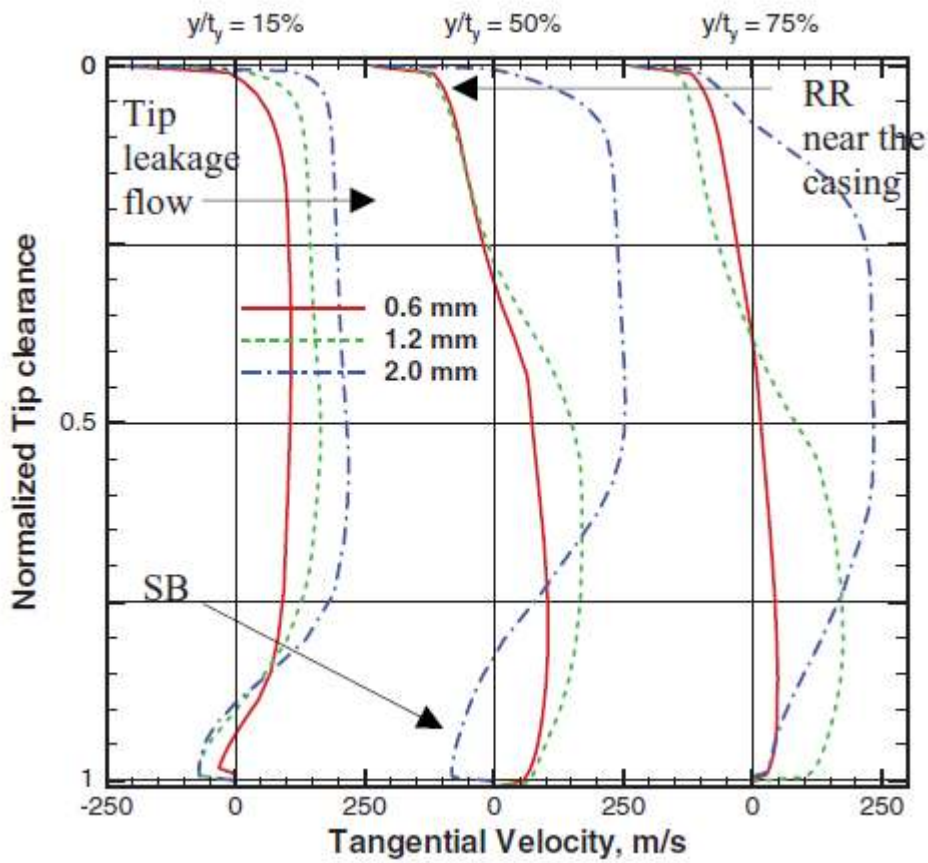
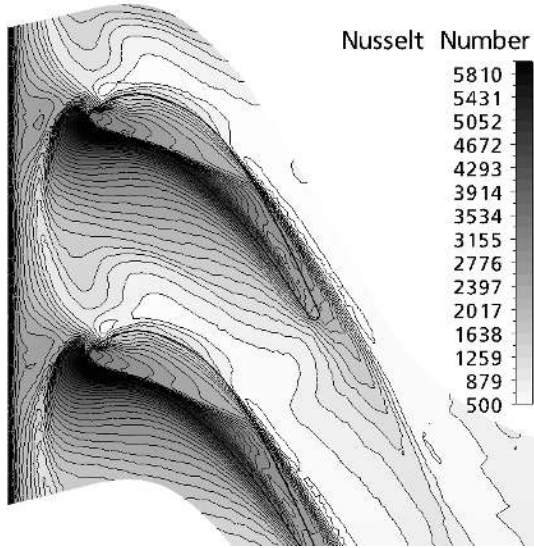
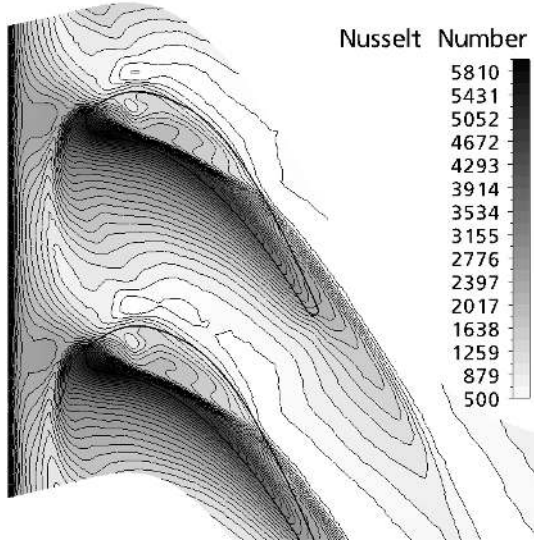


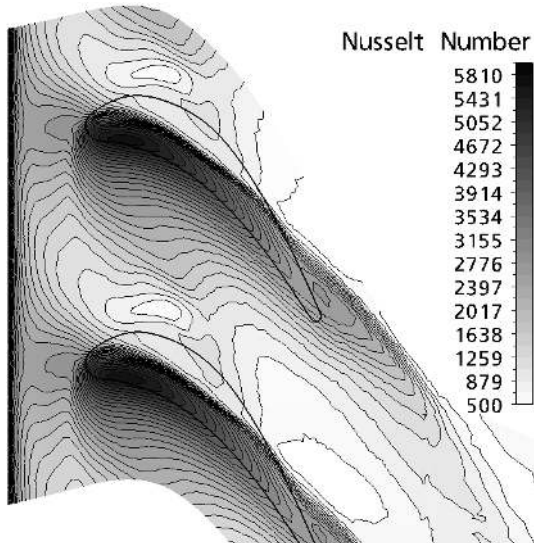
Figure 8. Tangential velocity profiles along the thickness at the 25% axial chord for different clearance heights.



(a) Case 1 (0.6 mm)



(b) Baseline (1.2mm)



(c) Case 2 (2 mm)

Figure 9. Contours of predicted Nusselt number on the shroud for three different clearance heights.

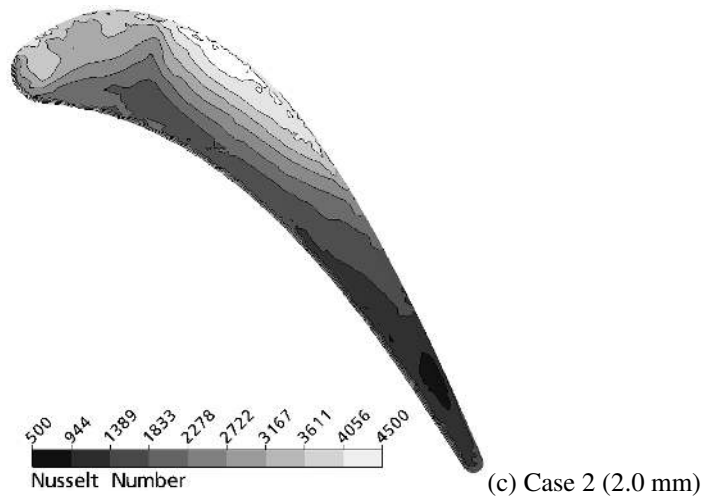
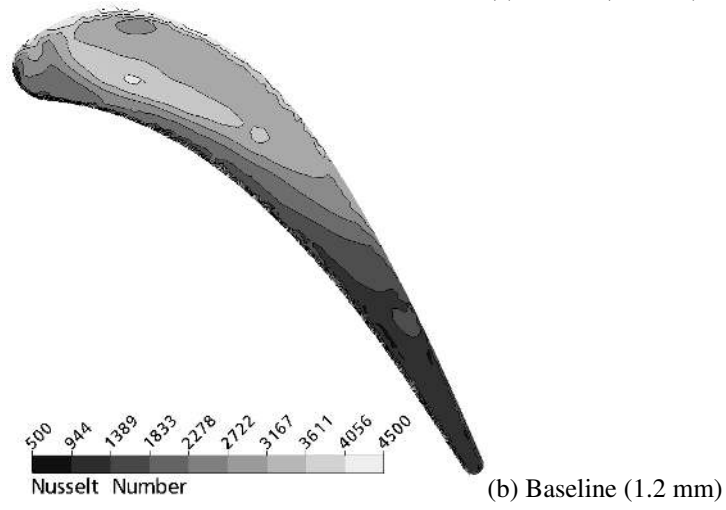
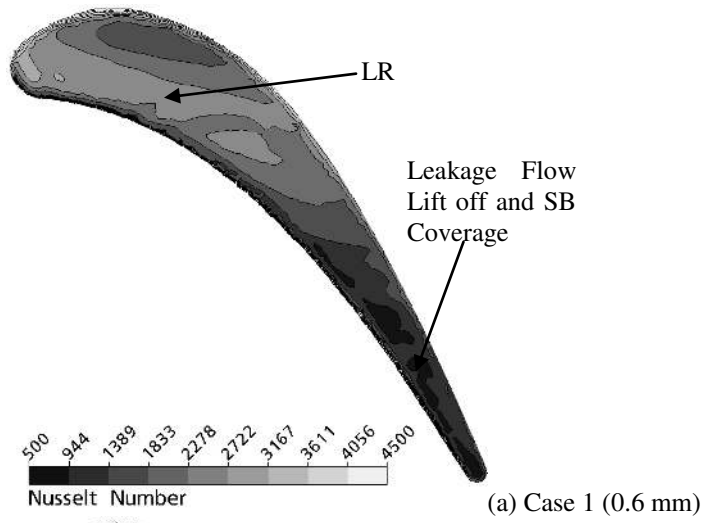


Figure 10. Contour of predicted Nusselt number on the blade tip surface for different height of the clearance.

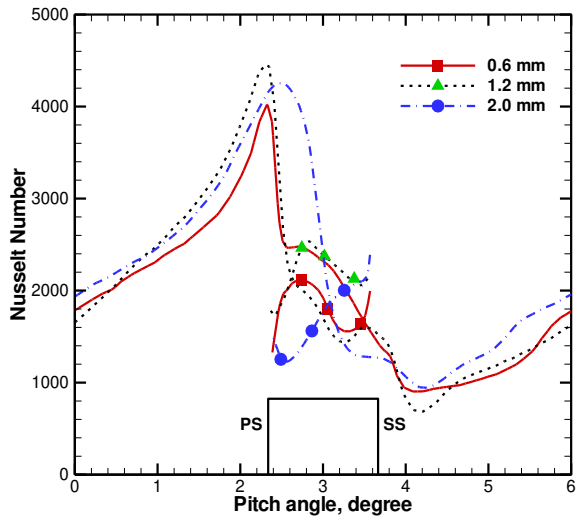


Figure 11. Nusselt number distributions along the casing circumference at the 25% axial chord plane for different clearance heights.

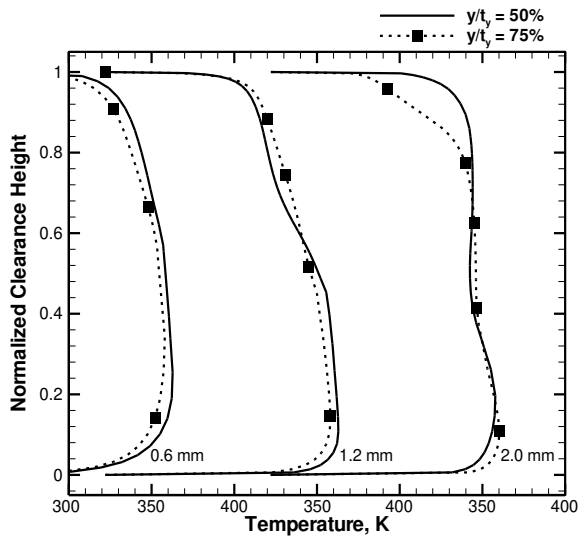
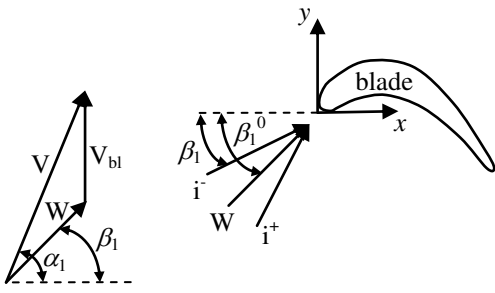
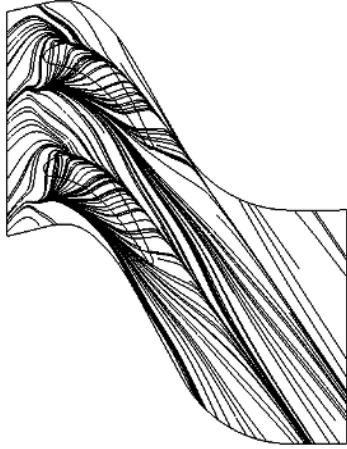


Figure 12. static temperature profile along the y-direction at the 25% axial chord for different clearance heights.



(a) Velocity triangle and incidence angle



(b) Baseline (9500 RPM)



(c) Case 3 (12500 RPM)



(d) Case 4 (15500 RPM)

Figure 13. Streamlines over the blade tip for three different speeds.

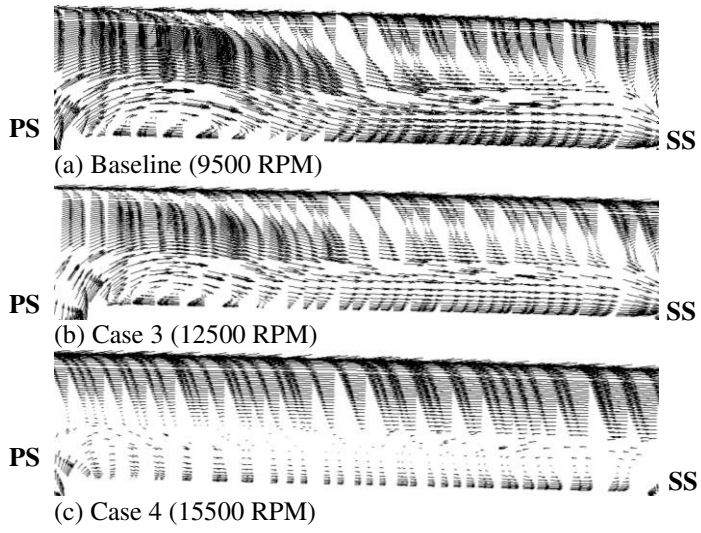
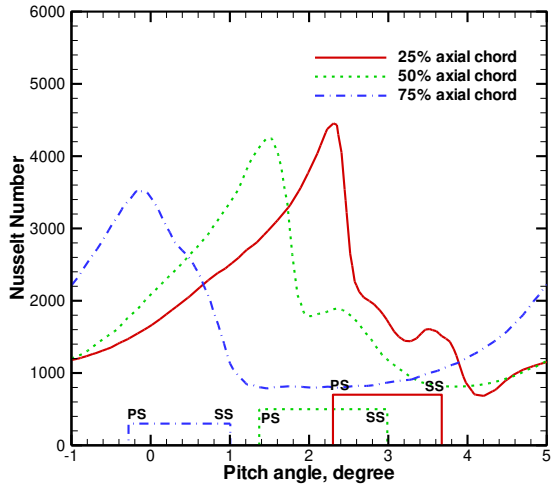
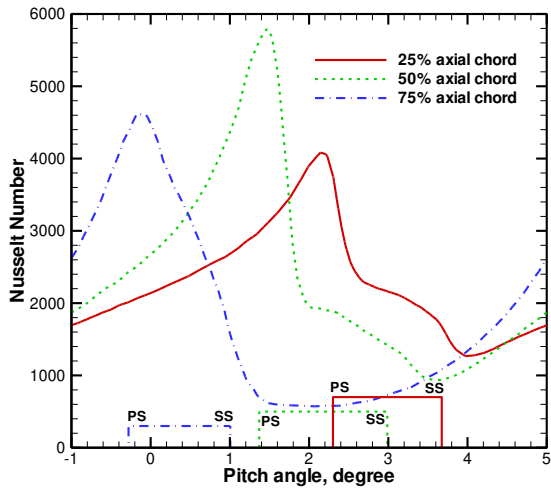


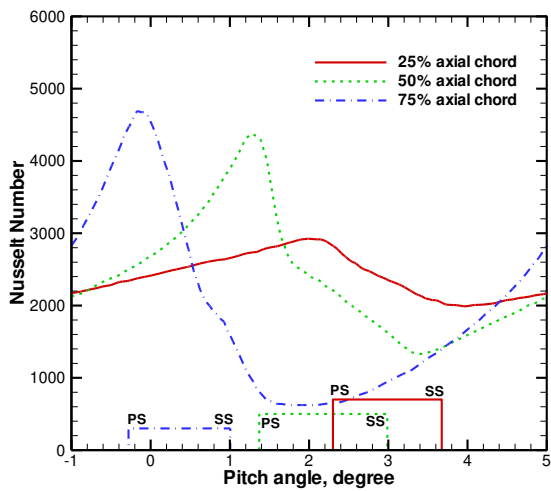
Figure 14. 2D velocity vectors at the quarter axial chord plane.



(a) Baseline (9500 RPM)



(b) Case 3 (12500 RPM)



(c) Case 4 (15500 RPM)

Figure 15. Nusselt number distribution along casing circumference from line of projections of blade tip pressure to suction.

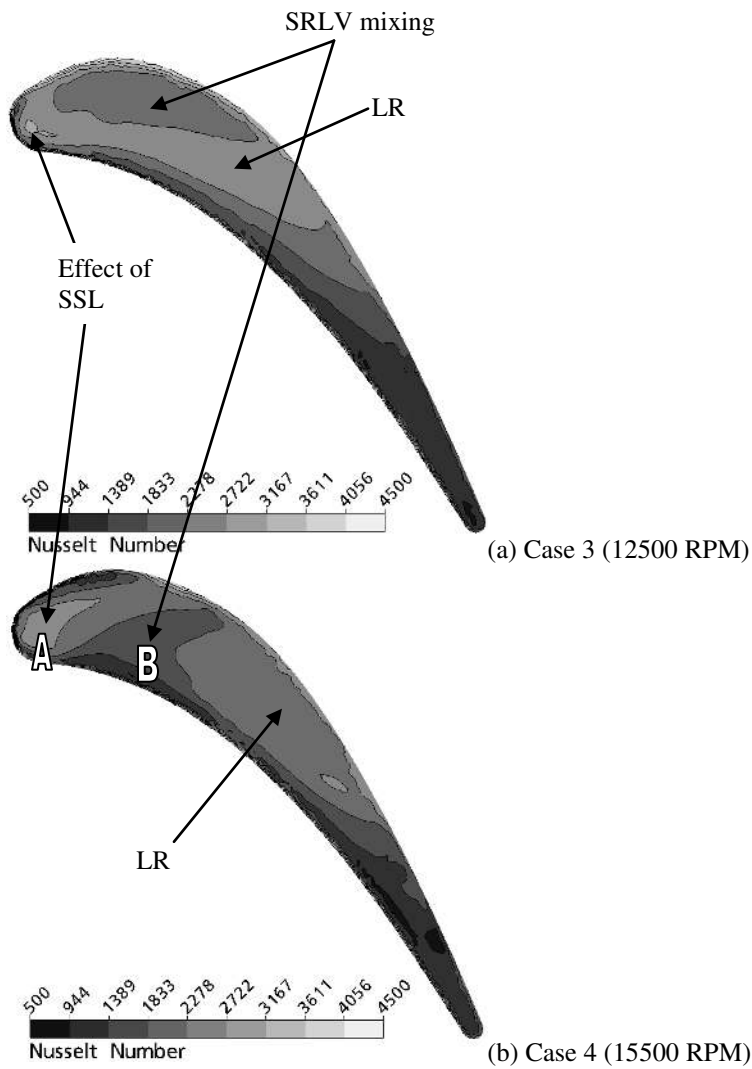


Figure 16. Contour of Nusselt number on the blade tip surface for different speeds.

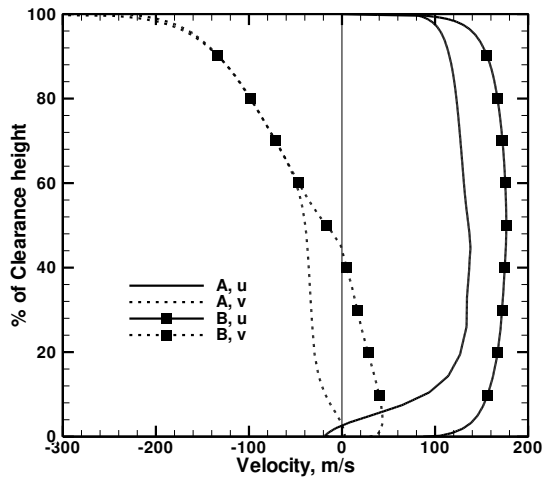


Figure 17. U and V velocity profile in the locations indicated in Fig. 16b.

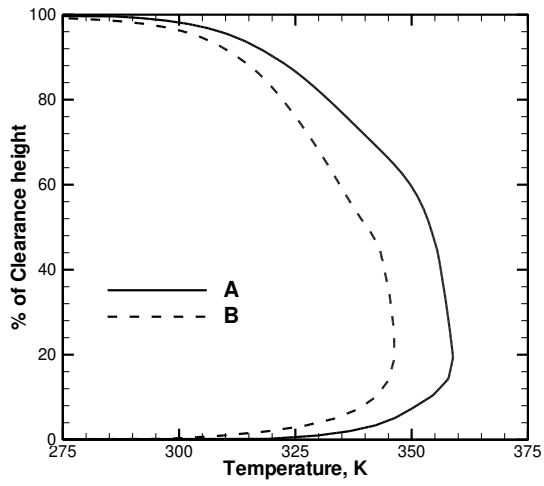


Figure 18. Temperature profile in the locations indicated in Fig. 16b.